Manipulation of instabilities in core-annular flows using a deformable solid layer

Gaurav and V. Shankar

Citation: Phys. Fluids **25**, 014104 (2013); doi: 10.1063/1.4788712
View online: http://dx.doi.org/10.1063/1.4788712
View Table of Contents: http://pof.aip.org/resource/1/PHFLE6/v25/i1
Published by the American Institute of Physics.

PHYSICS OF FLUIDS **25**, 014104 (2013)

Manipulation of instabilities in core-annular flows using a deformable solid layer

Gaurav[a] and V. Shankar[b]
Department of Chemical Engineering, Indian Institute of Technology, Kanpur 208 016, India

(Received 28 August 2012; accepted 20 December 2012; published online 29 January 2013)

The stability of core-annular flow (CAF) of two immiscible fluids surrounded by a soft, deformable solid layer is analyzed to examine the role of solid deformability on the interfacial instabilities in the CAF, using both low-wavenumber asymptotic analysis and numerical solutions by considering axisymmetric perturbations. For CAF in a rigid tube, two qualitatively distinct mechanisms due to capillary forces and viscosity stratification destabilize the interface between the two fluids. We show using a low-wavenumber analysis that the deformability of the solid layer has a stabilizing effect when the more viscous liquid is in the annular region, while it is destabilizing when the less viscous fluid is in the annular region. When the more viscous fluid is in the annulus, our numerical results demonstrate that by tuning the shear modulus of the solid layer, it is possible to maintain a stable core-annular flow (otherwise unstable in a rigid tube), where perturbations with all wavelengths are stable. For the same configuration, when the radius of the core fluid becomes small, we also find that it is possible to restrict the length scale of the instability to a small band of wavelengths. When the less viscous fluid is in the annulus, we show that the CAF (otherwise stable in a rigid tube) could be destabilized by solid deformability. Both these predictions, viz., suppression or enhancement of instability of the liquid-liquid interface by wall deformability could be potentially exploited in microfluidic drop formation applications that seek to control and manipulate the instability of the interface.
 [http://dx.doi.org/10.1063/1.4788712]

I. INTRODUCTION

Core-annular flows (CAF) are concentric flows of two immiscible fluids in a cylindrical geometry, with one cylindrical fluid layer flowing in the center of the tube and the other fluid in the surrounding annular region. Such flows have been studied extensively[1,2] in the context of lubricated pipe-lining, wherein the more viscous oil forms the core and the less viscous (and much thinner) water layer in the annulus, leading to lower pressure drops during transportation. Core-annular flows are also important in the context of liquid lining flows in lung airways,[3–5] where if the surface tension is sufficiently strong, the interface becomes unstable causing the liquid to block the air passage. Recently, core-annular flows are extensively investigated in the context of microfluidic devices involved in the controlled formation and manipulation of tiny mono-disperse droplets of volumes in the nanoliter regime.[6–9] Mono-disperse nanoliter-sized droplets are used in the preparation of double-emulsions,[10] colloidal nanoparticles of uniform size, and in micro-scale chemical synthesis within the droplets.[11] An important aspect in all these applications is the issue of stability of the core-annular flow, and its possible manipulation and control. In lubricated pipe-lining, for example, it is desired to prevent instabilities and maintain the core-annular nature of the flow in the pipeline. In contrast, in microfluidic droplet generation, the instability driven by capillarity is responsible for the creation of drops from a jet, and it would be desirable to have control on the onset instability, for

[a]Present address: Department of Chemical Engineering, Indian Institute of Technology, Roorkee, India.
[b]Author to whom correspondence should be addressed. Electronic mail: vshankar@iitk.ac.in.

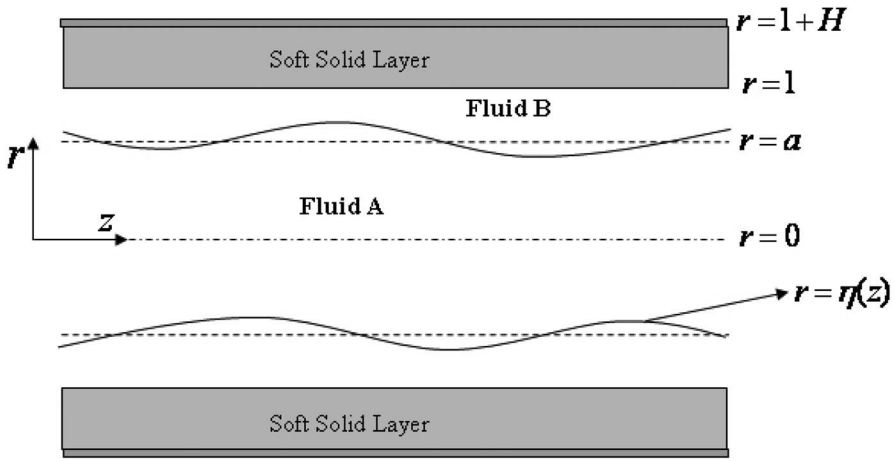

FIG. 1. Schematic diagram of the core-annular flow configuration and nondimensional coordinate system studied in this paper.

example, by initiating the breakup of the jet at a specific position in the channel. Previous studies have examined the role of geometric confinement,[12] or the presence of interfacial surfactants[13–16] on the suppression or enhancement of the capillary instability. In the present study, we study the role of a soft, deformable solid layer coating (surrounding the annular fluid layer; Figure 1), on the instability of the interface in a core-annular flow. This configuration is particularly relevant to microfluidics, where the silicone elastomer poly(dimethylsiloxane) (PDMS) is often used as the material in the soft-lithographic fabrication of sub-millimeter sized channels.[17] In this paper, we demonstrate using asymptotic analysis and numerical solutions that the deformability of the soft solid layer has a profound influence on the capillary instability in a core-annular flow. This result suggests that it is possible to manipulate the formation of droplets by delaying the onset of instability or by enhancing it by tuning the shear modulus of the PDMS elastomer. In the remainder of the Introduction, we briefly review relevant earlier work, and motivate the context for the present study.

A quiescent fluid cylinder surrounded by another fluid is unstable because axisymmetric perturbations to the interface with wavelengths larger than its perimeter tend to decrease its interfacial area (and consequently, the interfacial energy) at constant volume. This phenomenon was addressed by Rayleigh[18,19] who treated the liquid as inviscid, and this instability is referred to as the capillary instability. This phenomenon is also observed in the uniform flow of a liquid jet surrounded by gas, since one could transform this system to a quiescent fluid state by using a Galilean transformation using a moving frame of reference. The interfacial tension acts to enhance azimuthal curvature, while stabilizing the curvature in the axial direction of the jet. The unstable mode with the largest growth rate has a wavelength little larger than the perimeter of the jet. Tomotika[20] generalized this problem by treating the liquid jet to be viscous and surrounded by a different viscous liquid of infinite expanse. In this configuration, the maximum growth rate occurs for perturbations with infinitely large wavelengths when the viscosity of one of the liquids is negligible compared to the other. When the viscosity ratio of the two liquids is finite (i.e., neither zero nor infinity), the maximum growth rate occurs at finite wavelengths. This destabilizing nature of capillary forces on a cylindrical thread is present regardless of whether the fluid thread is quiescent, or is flowing in a core-annular configuration surrounded by another immiscible liquid inside a tube. However, the core-annular flow of two immiscible fluids with different viscosities is also characterized by a discontinuity of the base flow (radial) velocity gradients at the interface. This discontinuity leads to an instability due to "viscosity stratification" first predicted for planar two-layer flows by Yih.[21] Thus, in the CAF of two immiscible liquids, there are two qualitatively different mechanisms of destabilization, one due to the capillary stresses, and the other due to viscosity stratification. Hickox[22] analyzed the problem of stability of CAF, and found that when the more viscous fluid is in the annular region, the viscosity stratification is also destabilizing, when the annular fluid thickness is much smaller than the core fluid thickness.

When the core-fluid thickness is very small compared to the annular fluid, the viscosity stratification could be stabilizing. However, the destabilizing capillary forces are much stronger, and hence it is very unlikely to observe a stable CAF when the core fluid is less viscous than the annular fluid.

Joseph and co-workers[1,2,23] have carried out extensive studies in this area, and showed that when the more viscous fluid is in the core, and if the annular fluid thickness is small, then the viscosity stratification is stabilizing, while capillary effects are always destabilizing. At sufficiently large Reynolds number, they showed using long-wave analysis and numerical solutions that it is possible for the stabilizing nature of the viscosity stratification to overcome the destabilizing capillary forces, leading to a stable CAF configuration. A majority of the stability analyses have focused on the stability of CAF to axisymmetric (no θ-dependence) disturbances. A few studies[24–26] have also addressed the issue of non-axisymmetric disturbances, and concluded that non-axisymmetric modes are important if the core fluid is more viscous and of much less radius compared to the annular thickness. However, if the destabilization due to capillary forces is dominant (compared to the contribution from viscosity stratification), the most unstable modes are found to be axisymmetric. With lubricated pipe-lining as the primary goal, most papers in the literature have tended to focus on axisymmetric disturbances, and on the case where the annular fluid is very less viscous and very thin compared to the core fluid. A comprehensive review of the work related to lubricated pipe-lining and stability of core-annular flows can be found in the monograph by Joseph and Renardy[1] and the review paper by Joseph *et al.*[2] Halpern and Grotberg[4,5] analyzed the problem of the stability of an annular liquid layer that is coated inside a flexible tube (with the core region being filled with air), as a model for closure of small airways of the lungs. The flexible tube is modelled as a thin membrane with tension and bending forces, that deforms only in the normal direction. However, the annular liquid layer was stationary in their analysis, in contrast to the studies in core-annular flow. They studied the role of the wall flexibility on the capillary instability, but the flexible membrane itself was free to deflect and collapse. This situation is different from the microfluidic context, where the deformable solid is of finite thickness and is typically bonded to another rigid substrate.

A number of studies have also analyzed the effect of surfactants at the interface on the capillary instability in a core-annular flow.[13–15] It might be expected that the addition of surfactants will decrease the interfacial tension, and hence mitigate the capillarity-induced destabilization. While this intuitive expectation holds for quiescent fluids to some extent,[27] the presence of a core-annular flow leads to a nonzero interfacial velocity, which gives rise to a new Marangoni-like destabilization of the interface. Very recently, Bassom *et al.*[16] studied the stability of a core-annular flow that surrounds a cylindrical solid rod, and showed that the presence of interfacial surfactants can stabilize the flow even at zero Reynolds number, by tuning the shear rate of the base flow at the liquid-liquid interface. They used asymptotic analysis when either one of the two fluids is thin compared to the total thickness of the two fluids, and showed that for a thin inner layer the flow is stabilized if the inner liquid is more viscous. The role of miscibility of the two fluids was examined by Selvam *et al.*[28] who showed that the finite nature of the "interfacial" zone leads to stabilization. However, the diffusion of the miscible species between the two phases leads to destabilization.

Recently, there has been also a lot of interest in determining the conditions under which the instability of a core-annular flow would be convective or absolute. If the instability is absolute, then the core fluid immediately breaks up into drops after ejecting from the nozzle. In contrast, if the instability is convective, then a more continuous fluid thread would persist along the flow geometry. Utada *et al.*[7,8] carried out experiments to identify the flow regimes under which the two different regimes would exist in a core-annular flow. Ajdari and co-workers[9,29] have carried out experiments and a lubrication-theory based analysis to characterize convective and absolute nature of the instability in a microfluidic core-annular flow. Humphry *et al.*[12] showed that instabilities in the flow of two immiscible fluids in a rectangular microfluidic channel can be suppressed by geometric confinement. By making the channel width comparable to the channel height, they showed that the interfacial instabilities can be suppressed and the jet remains stable. They also showed that changing the nature of confinement along the flow direction could result in drop formation at a desired location in the geometry.

In the present study, we propose and evaluate a different strategy for manipulation of instabilities in a core-annular flow, by examining the effect of a soft, deformable solid coating that surrounds the

annular liquid layer on the interfacial instability. When there is fluid flow adjacent to a soft solid layer, the dynamics of the fluid is coupled to the deformation in the solid, and this elastohydrodynamic coupling is known to lead to the instability of the interface between the fluid and the soft solid.[30–33] In our earlier work, we have addressed the problem of planar two-layer flows past a soft solid layer,[34–38] and have shown that when the solid layer is sufficiently deformable, the interfacial instability due to viscosity stratification (the so-called "Yih mode"[21]) can be completely suppressed at all wavelengths, without triggering the instability at the interface between the liquid and the gel. In the present study, we generalize those studies to the case of a core-annular flow, where, in addition to the viscosity-stratification induced instability there is also the capillary instability due to the cylindrical nature of the core fluid flow. The destabilizing nature of the capillary instability is dominant even in the presence of the flow. Hence, it is of interest to examine whether the stabilizing nature of the deformable solid layer is present even in core-annular flows. If the deformable solid coating is able to alter the stability characteristics, by either suppressing the instability in a core-annular flow or by enhancing it, this could be potentially exploited in microfluidic devices that are fabricated using PDMS. For example, one could imagine making a PDMS device with a spatially varying (along the flow direction) elastic modulus (for example, by varying the cross-linking in the gel), to have control on the location of the onset of the instability. However, at the same time, care must be taken to ensure that flow-induced instabilities in a deformable tube[39,40] are not excited when the solid layer is made deformable. We address both these issues in our following analysis, by using both asymptotic methods and numerical solutions.

The rest of the paper is structured as follows: In Sec. II, we formulate the problem and provide the equations governing the fluid flow and the wall deformation in Sec. II A. In Sec. II C, we formulate the linearized equations and boundary conditions that govern the stability of the system. In Sec. III, we discuss the results from a long-wave asymptotic analysis to show the effect of the solid layer on the stability of the core-annular flow. Section IV provides a discussion of the numerical results obtained at arbitrary wavenumbers. Section V provides the key conclusions of the present work.

II. PROBLEM FORMULATION

The system consists of two concentric, immiscible, incompressible Newtonian liquids flowing axisymmetrically in a core-annular arrangement in a deformable tube of inner radius R_2 and outer radius $(1 + H)R_2$ as shown in Figure 1. At the outer surface, the deformable solid layer is assumed to be perfectly bonded to a rigid tube. The deformable solid medium is modeled as impermeable and incompressible neo-Hookean viscoelastic solid[41–43] of density ρ, shear modulus G, and viscosity η_s. The core-liquid (liquid A with viscosity μ_a) occupies a region $0 \le r^* \le R_1$ and the annular liquid (liquid B with viscosity μ_b) occupies a region $R_1 \le r^* \le R_2$ in the unperturbed base state. The densities of deformable solid wall medium and both liquids are assumed to be identical and are denoted by ρ. Various physical quantities are nondimensionalized at the outset by using following scales: R_2 for lengths and deformations, center-line velocity $V = P^*\left(\frac{R_1^2(\mu_b-\mu_a)+R_2^2\mu_a}{4\mu_a\mu_b}\right)$ for velocities, and $\frac{\mu_b V}{R_2}$ for pressure and stresses. The dimensional pressure gradient driving the steady base flow of both the liquids is given by $P^*\mathbf{e}_z = -\nabla^* p^*$.

A. Governing equations

The non-dimensional equations governing the two liquid layers are the Navier-Stokes continuity and momentum equations

$$\nabla \cdot \mathbf{v}^\alpha = 0, \tag{1}$$

$$Re^\alpha[\partial_t \mathbf{v}^\alpha + \mathbf{v}^\alpha \cdot \nabla \mathbf{v}^\alpha] = -\nabla p^\alpha + \mu_{\mathrm{r}}^\alpha \nabla \cdot \mathbf{T}^\alpha. \tag{2}$$

Here, $\mathbf{v}^\alpha$ and p^α are the velocity and pressure fields in liquid $\alpha = a, b$; $\mu_{\mathrm{r}}^\alpha = \mu_{\mathrm{r}} = \mu_a/\mu_b$ for liquid A ($\alpha = a$) and $\mu_{\mathrm{r}}^\alpha = 1$ for liquid B ($\alpha = b$); $\mathbf{T}^\alpha = \mu_{\mathrm{r}}^\alpha[\nabla \mathbf{v}^\alpha + (\nabla \mathbf{v}^\alpha)^T]$ is the Cauchy stress tensor

for liquid α ($=a$ or b) and $Re = \frac{\rho V R_2}{\mu_b}$ is the Reynolds number based on the viscosity of the annular liquid B.

The governing equations for the liquid layers above are written in terms of spatial (Eulerian) coordinates ($\mathbf{x} = r, \theta, z$), while it is convenient (following the earlier work of Gkanis and Kumar[32]) to refer the governing equations for the solid in terms of a reference (Lagrangian) configuration, where the independent variables are the spatial positions $\mathbf{X} = (R, \Theta, Z)$ of material particles in the reference (i.e., unstressed) configuration. Thus, the spatial (r, θ, z) coordinate system used for fluid motion is identical to the reference coordinates (R, Θ, Z) in the unstressed configuration for the deformable solid. In the deformed state of the solid, the spatial positions of the material particles are denoted by $\boldsymbol{w}(\mathbf{X})$, where $\boldsymbol{w} = (w_R, w_\Theta, w_Z)$. The deformable solid is modeled as an incompressible neo-Hookean viscoelastic solid and the mass and momentum conservation equations governing the dynamics of solid are given as[44,45]

$$\det(\mathbf{F}) = 1, \tag{3}$$

$$Re\left[\frac{\partial^2 \boldsymbol{w}}{\partial t^2}\right]_{\mathbf{X}} = \nabla_X \cdot \mathbf{P}, \tag{4}$$

where the subscript $\mathbf{X}$ on a partial derivative implies that the derivative is taken with the material particle position being kept constant (i.e., Lagrangian derivative), and $\mathbf{X}$ is the Lagrangian position of a material particle in the unstressed configuration. In the above equations, $\mathbf{F}$ is the deformation gradient tensor defined as $\mathbf{F} = \nabla_{\mathbf{X}} \boldsymbol{w}$ and $\mathbf{P}$ is the first Piola-Kirchhoff stress tensor. The first equation (3) is an expression of incompressibility of the solid, while the second equation (5) is the Cauchy momentum equation for a solid.[44] The first Piola-Kirchhoff stress tensor is related to Cauchy stress tensor by $\mathbf{P} = \mathbf{F}^{-1} \cdot \boldsymbol{\sigma}$. The Cauchy stress tensor for neo-Hookean viscoelastic solid is split into an elastic part, $\boldsymbol{\sigma}_e$, and a dissipative part, $\boldsymbol{\sigma}_d$[41–43]

$$\boldsymbol{\sigma} = \boldsymbol{\sigma}^e + \boldsymbol{\sigma}^d, \tag{5}$$

$$\boldsymbol{\sigma}^e = -p_s \mathbf{I} + \frac{1}{\Gamma}\mathbf{F} \cdot \mathbf{F}^T, \quad \boldsymbol{\sigma}^d = \eta_r(\boldsymbol{L} + \boldsymbol{L}^T), \tag{6}$$

where p_s is the pressure-like function related to actual pressure, $\hat{p}_s$, in the neo-Hookean solid as $p_s = \hat{p}_s + \frac{1}{\Gamma}$, $\mathbf{L} = \dot{\mathbf{F}} \cdot \mathbf{F}^{-1}$ is the spatial velocity gradient, overdots represent material time derivatives, and $\eta_r = \eta_s/\mu_b$ is the ratio of solid to annular fluid viscosity. Here, $\Gamma = \mu_b V/GR_2$ is the ratio of viscous shear stresses in liquid B to elastic stresses in the solid medium. The parameter Γ is a measure of deformability of the solid medium and $\Gamma \to 0$, in the limit of a rigid solid.

B. Base state

The laminar base velocity profiles in the core and annular liquid layers consist of unidirectional flow in z-direction driven by a uniform pressure gradient. In the base-state, the liquid-liquid (LL) and liquid-solid (LS) interfaces are perfectly axisymmetric and cylindrical, and are located at non-dimensional mean radii $r = a(=R_1/R_2)$ and $r = 1$, respectively. The overbar in the following equations denote various base-state quantities. The non-dimensional base velocity profiles in the two liquid layers are

$$\overline{v}_z^a = 1 - \frac{r^2}{\mu_\mathrm{r} + a^2(1 - \mu_\mathrm{r})} \quad \text{for} \quad 0 \le r \le a, \tag{7}$$

$$\overline{v}_z^b = \frac{\mu_\mathrm{r}(1 - r^2)}{\mu_\mathrm{r} + a^2(1 - \mu_\mathrm{r})} \quad \text{for} \quad a \le r \le 1. \tag{8}$$

The deformable solid wall of the tube is at rest in this steady state with a nonzero displacement in z-direction due to shear stress exerted by liquid B at the LS interface. The deformation and pressure

fields in the solid wall ($1 \le r \le 1 + H$) are given as

$$\overline{w}_Z = Z + \frac{\Gamma P}{4}\left[(1+H)^2 - R^2\right], \quad \overline{w}_R = R, \tag{9}$$

$$\overline{p}_s = \overline{p}^b(z) + \frac{\Gamma P^2}{4}(R^2 - 1) - \Sigma_1. \tag{10}$$

In the above equations, $\Sigma_1 = \gamma_1/\mu_b V$ is the non-dimensional interfacial tension at LS interface with γ_1 being the dimensional LS interfacial tension, and $P = \frac{4\mu_r}{\mu_r + a^2(1-\mu_r)} = -\nabla\overline{p}^\alpha$ is the non-dimensional pressure gradient. The neo-Hookean solid also exhibits a jump in first normal stress difference in base state: $\overline{\sigma}_{RR} - \overline{\sigma}_{ZZ} = -\frac{\Gamma P^2 R^2}{4}$ which gives rise to a high wavenumber instability at the LS interface.[32]

C. Linearized governing equations and interface conditions

A standard temporal linear stability analysis is performed in order to determine the stability of pressure-driven core-annular flow in a deformable neo-Hookean viscoelastic tube. Only axisymmetric disturbances are considered in the present study, as they are usually the most dangerous modes for core-annular flow in a rigid tube.[22,23] As pointed out in the Introduction, Hu and Patankar[25] show that when the capillary destabilizing forces are dominant compared to viscosity-stratification, then the unstable modes are axisymmetric. The perturbed quantities are expressed using the standard normal mode decomposition as

$$(v_r{}', w_R{}') = (\mathrm{i}\tilde{v}_r^\alpha(r), \mathrm{i}\tilde{w}_R(R))\exp[\mathrm{i}k(z - ct)]$$

for normal velocity and normal displacement fluctuations and $f' = \tilde{f}(r)\exp[\mathrm{i}k(z - ct)]$ for fluctuations to all other dynamical variables. Here, $\tilde{f}(r)$ is the complex amplitude function of the disturbance, k is the stream-wise wavenumber of perturbations, and $c = c_r + \mathrm{i}c_i$ is the complex wavespeed. For the deformable solid wall, r and z are replaced by R and Z. If $c_i > 0$ (or $c_i < 0$), flow will be unstable (or stable). The linearized governing equations for the core and annular liquid layers, with $\mathrm{d}_r \equiv \mathrm{d}/\mathrm{d}r$, are

$$\mathrm{d}_r\tilde{v}_r^\alpha + \frac{1}{r}\tilde{v}_r^\alpha + k\tilde{v}_z^\alpha = 0, \tag{11}$$

$$\mathrm{i}Re[k\tilde{v}_z^\alpha(\overline{v}_z^\alpha - c) + \tilde{v}_r^\alpha \mathrm{d}_r\overline{v}_z^\alpha] = -\mathrm{i}k\tilde{p} + \mu_r^\alpha(\mathrm{d}_r^2 + \frac{1}{r}\mathrm{d}_r - k^2)\tilde{v}_z^\alpha, \tag{12}$$

$$-kRe(\overline{v}_z^\alpha - c)\tilde{v}_r^\alpha = -\mathrm{d}_r\tilde{p} + \mathrm{i}\mu_r^\alpha(\mathrm{d}_r^2 + \frac{1}{r}\mathrm{d}_r - \frac{1}{r^2} - k^2)\tilde{v}_r^\alpha, \tag{13}$$

and the governing stability equations for deformable wall of the tube are

$$\mathrm{d}_R\tilde{w}_R + \frac{1}{R}\tilde{w}_R + k\tilde{w}_Z + \frac{\Gamma Pr}{2}\mathrm{i}k\tilde{w}_R = 0, \tag{14}$$

$$\begin{aligned} -k^2c^2Re\,\tilde{w}_Z = &-\left(\frac{P^2}{2}k\Gamma R\tilde{w}_R - \mathrm{i}P\mathrm{d}_R\tilde{w}_R - \mathrm{i}P\frac{\tilde{w}_R}{R}\right) - \mathrm{i}k\tilde{p}_s \\ &+\left(\frac{1}{\Gamma} - \mathrm{i}kc\eta_r\right)\left(\mathrm{d}_R^2 + \frac{1}{R}\mathrm{d}_R - k^2\right)\tilde{w}_Z \\ &-\mathrm{i}k^2c\eta_r\Gamma P\left(\mathrm{i} - \frac{k\Gamma PR^2}{4} + \mathrm{i}R\,\mathrm{d}_R\right)\tilde{w}_Z, \end{aligned} \tag{15}$$

$$-k^2c^2Re\,\tilde{w}_R = -P\left(\frac{k\Gamma PR}{2}\tilde{w}_Z + \frac{k\Gamma R}{2}\tilde{p}_s - \mathrm{i}\mathrm{d}_R\tilde{w}_Z\right) + \mathrm{i}\mathrm{d}_R\tilde{p}_s + \left(\frac{1}{\Gamma} - \mathrm{i}kc\eta_r\right)\left(\mathrm{d}_R^2 + \frac{1}{R}\mathrm{d}_R - \frac{1}{R^2} - k^2\right)\tilde{w}_R + k^2c\eta_r\Gamma PR\left(\mathrm{d}_R + \frac{1}{R} + \frac{\mathrm{i}k\Gamma PR}{4}\right)\tilde{w}_R. \tag{16}$$

The conditions at perturbed liquid-liquid interface (denoted by $r = a + \eta(z, t)$) are continuity of velocities and stresses along with the kinematic condition for the evolution of LL interface. A Taylor expansion about the unperturbed LL interface is used to express the dynamical variables at perturbed LL interface in terms of quantities at unperturbed LL interface. The linearized kinematic, velocity and stress conditions at $r = a$ are

$$\tilde{\eta}k(\overline{v}_z^a(r=a) - c) = \tilde{v}_r^a(r=a), \tag{17}$$

$$\tilde{v}_r^a = \tilde{v}_r^b, \tag{18}$$

$$\tilde{v}_z^a + \tilde{\eta}\,\mathrm{d}_r\overline{v}_z^a = \tilde{v}_z^b + \tilde{\eta}\,\mathrm{d}_r\overline{v}_z^b, \tag{19}$$

$$\mu_r(\mathrm{d}_r\tilde{v}_z^a - k\tilde{v}_r^a) = (\mathrm{d}_r\tilde{v}_z^b - k\tilde{v}_r^b), \tag{20}$$

$$-\tilde{p}^a + 2\mathrm{i}\,\mu_r\,\mathrm{d}_r\tilde{v}_r^a = -\tilde{p}^b + 2\mathrm{i}\,\mathrm{d}_r\tilde{v}_r^b + \frac{\tilde{\eta}\Sigma}{a^2}(1 - k^2a^2). \tag{21}$$

Here, $\Sigma = \gamma/\mu_b V$ is the non-dimensional LL interfacial tension with γ being the dimensional surface tension at LL interface. While the Eulerian description is used for both core and annular liquids, a Lagrangian framework is used to express the dynamical variables of the deformable solid wall. Thus, the treatment of interfacial conditions at perturbed LS interface is different as compared to conditions at LL interface, and is discussed in detail in Gaurav and Shankar.[46] As explained in our earlier work, Taylor-series expansion is not required to evaluate any solid variable on the perturbed interface in the Lagrangian description of solid. The conditions at liquid-solid interface are continuity of velocities and stresses in annular liquid B and the deformable wall of the tube. Following the procedure described in Ref. 46, the linearized conditions at unperturbed LS interface ($r = 1$ or $R = 1$) are

$$\tilde{v}_r^b = -\mathrm{i}kc\tilde{w}_R, \tag{22}$$

$$\tilde{v}_z^b + \mathrm{i}\tilde{w}_R\,\mathrm{d}_r\overline{v}_z^b = -\mathrm{i}kc\tilde{w}_Z, \tag{23}$$

$$(\mathrm{d}_r\tilde{v}_z^b - k\tilde{v}_r^b) = \left(\frac{1}{\Gamma} - \mathrm{i}kc\eta_r\right)(\mathrm{d}_R\tilde{w}_Z - k\tilde{w}_R) + \frac{\Gamma P^2}{4}k\tilde{w}_R - \frac{\mathrm{i}P}{2}\mathrm{d}_R\tilde{w}_R - \frac{k^2c\eta_r\Gamma P}{2}\tilde{w}_Z - \mathrm{i}\tilde{w}_R(\mathrm{d}_r^2\overline{v}_z^b), \tag{24}$$

$$-\tilde{p}^b + 2\mathrm{i}\,\mathrm{d}_r\tilde{v}_r^b = -\tilde{p}_s + 2\mathrm{i}\left(\frac{1}{\Gamma} - \mathrm{i}kc\eta_r\right)\mathrm{d}_R\tilde{w}_R \quad \mathrm{i}k^2c\eta_r\Gamma P\tilde{w}_R + \mathrm{i}\Sigma_1\tilde{w}_R(1 - k^2). \tag{25}$$

The velocities and pressure are finite at the center of the tube ($r = 0$) and finally, the boundary conditions at rigid surface ($r = 1 + H$) are no deformation conditions

$$\tilde{w}_R = 0, \quad \tilde{w}_Z = 0. \tag{26}$$

This completes the description of linearized governing equations and interfacial conditions. The stability of the composite system is determined by solving Eqs. (11)–(26) for eigenvalue c as a function of k, Re, Γ, H, η_r, μ_r, a, Σ, and Σ_1. A pseudo-spectral collocation method[47–49] and a numerical shooting procedure[50] are used to numerically evaluate the eigenvalues and neutral stability boundaries. The details of implementation of pseudo-spectral methods to two-phase flows was given by Boomkamp *et al.*[51] Results from our computer codes were bench-marked with the earlier results of Hickox[22] and Preziosi *et al.*[23] for CAF in a rigid tube, and very good agreement was found with earlier results.

III. LONG-WAVE ASYMPTOTIC ANALYSIS

In a rigid tube, the interface between core and annular liquids is susceptible to long-wave capillary instability for nonzero values of interfacial tension. Further, depending on the viscosity ratio and the ratio of core to tube radius, the liquid-liquid interface could also become unstable for long-wave disturbances due to viscosity contrast across the interface.[22,23] The long-wave instability of core and annular liquid interface will be referred here as the LL mode interfacial instability. We have performed a long-wave (or, low wavenumber $k \ll 1$) asymptotic analysis to examine the effect of deformability of the tube wall on the LL interface which could undergo an instability due to capillary forces and/or viscosity contrast. The details of the calculation are quite similar to the earlier works by Yih,[21] Hickox,[22] and Preziosi *et al.*[23] for rigid surfaces, and to our earlier works on the role of wall deformability on planar two-layer flows.[34,35] Here, we provide a brief outline of the qualitatively new features of the analysis.

For $k \ll 1$, the complex wavespeed is expanded in an asymptotic series in k: $c = c^{(0)} + kc^{(1)} + \cdots$. The velocity and displacement fields in the two fluids and the solid are also expanded in an asymptotic expansion in k. For example, the $r-$component of the velocity field in liquid B is expanded as

$$\tilde{v}_r^b = \tilde{v}_r^{b(0)} + k\tilde{v}_r^{b(1)} + \cdots. \tag{27}$$

From the continuity equation (11), the z-component velocity $\tilde{v}_z^b$ is $O(k^{-1})$ larger than $\tilde{v}_r^b$, and hence $\tilde{v}_z^b$ is expanded as

$$\tilde{v}_z^b = k^{-1}\tilde{v}_z^{b(0)} + \tilde{v}_z^{b(1)} + \cdots. \tag{28}$$

The z-momentum equation (12) yields the expansion for the pressure as $\tilde{p}^{(b)} = k^{-2}\tilde{p}^{b(0)} + k^{-1}\tilde{p}^{b(1)} + \cdots x$. Similar expansions hold for fluid A as well. The displacements in the solid layer are expanded as

$$\tilde{w}_R = \tilde{w}_R^{(0)} + k\tilde{w}_R^{(1)} + \cdots, \tag{29}$$

$$\tilde{w}_Z = k^{-1}\tilde{w}_Z^{(0)} + \tilde{w}_Z^{(1)} + \cdots, \tag{30}$$

$$\tilde{p}_s = k^{-2}\tilde{p}_s{}^{(0)} + k^{-1}\tilde{p}_s{}^{(1)} + \cdots. \tag{31}$$

After substituting these expansions in the governing equations, the solutions to the velocity fields in both the fluids, and the displacement field in the solid are obtained at each order of k analytically. It is sufficient to carry out the analysis up to $O(k)$ in c in order to discern the role of solid layer deformability in CAF. When the expansions are substituted in the linearized velocity and stress conditions at the liquid-solid interface (Eqs. (22)–(25)), it emerges that both the velocity components $\tilde{v}_r^{b(0)}$ and $\tilde{v}_z^{b(0)}$ become zero at the interface (to leading order in k), since the solid displacement is multiplied by k in the velocity continuity conditions (Eqs. (22) and (23)). In other words, to leading order in k, fluid B satisfies no-slip boundary conditions as appropriate for a rigid tube. However, the tangential stress continuity condition (24) at the liquid-solid interface imparts a non-zero displacement in the solid layer at leading order

$$d_r\tilde{v}_z^{b(0)} = \frac{1}{\Gamma}d_R\tilde{w}_Z^{(0)}. \tag{32}$$

Since no-slip conditions are valid at leading order for the fluid, the system is identical at this order to CAF in a rigid tube, and hence the wavespeed $c^{(0)}$ is identical to what was found in the earlier work of Hickox.[22] Thus, deformability of the solid layer does not affect the wavespeed at leading order. As in the case of CAF in a rigid tube, $c^{(0)}$ is purely real, and the flow is neutrally stable at this order.

However, the displacements imparted at leading order in the solid layer affect the first correction to the fluid velocity components $\tilde{v}_z^{b(1)}$ and $\tilde{v}_r^{b(1)}$ (through the first correction to the velocity continuity conditions at the interface), and this implies that the first correction to the wavespeed $c^{(1)}$ will be affected by solid deformability (characterized by the parameter Γ). The destabilizing effect due to capillary forces, and the effect of viscosity stratification also appear at this order in k in the expression for c. Hence, the stability of CAF in a deformable tube is determined by a balance of the three effects: capillary stresses, viscosity stratification, and solid deformability.

The first correction to the wavespeed $c^{(1)}$ turns out to be purely imaginary, and the result for $c^{(1)}$ can be written as

$$c^{(1)} = \mathrm{i}(f_1(\mu_\mathrm{r}, a)Re + f_2(\mu_\mathrm{r}, a)\Sigma + f_3(\mu_\mathrm{r}, a, H)\Gamma). \tag{33}$$

The analytical expressions for f_1, f_2, and f_3 are provided in the Appendix. The first term in the right-hand-side of Eq. (33) is proportional to Re, and signifies the role of viscosity stratification. The second term in the right-side of Eq. (33) is proportional to Σ, and denotes the destabilizing role of surface tension. The last term proportional to Γ denotes the role of solid layer deformability on the interfacial mode. The limit of a rigid solid layer is given by $\Gamma \to 0$, and the above expression reduces to the results of Hickox[22] and Preziosi *et al.*[23] for CAF in rigid tubes. However, for a soft, deformable solid, Γ is finite, and our asymptotic results show that the sign of the term f_3 is negative for $\mu_r < 1$ (stabilizing) while it is positive for $\mu_r > 1$ (destabilizing). Since $c^{(1)}$ is purely imaginary, and instability occurs if the imaginary part of wavespeed is positive, the competition between the three terms in the brackets of Eq. (33) determines the stability of the system. The numerical values of the functions f_1, f_2, and f_3 for two different values of μ_r and radius ratio a are provided in Tables I and II.

Physically, the deformation field set up in the solid layer at leading order affects the first correction to the velocity in the fluid via the continuity conditions at the interface. This implies that the deformation in the solid layer drives a flow at $O(k)$ that tends to modify the effects of viscosity stratification and surface tension. The nature of flow driven by the solid deformation determines whether the role of the solid layer is stabilizing or destabilizing.

The key results of the low-k analysis are discussed next. We first consider the case when the annular liquid is more viscous than the core liquid (i.e., $\mu_\mathrm{r} < 1$). As a representative example of $\mu_\mathrm{r} < 1$, Table I gives the values of $c^{(0)}$ and expressions for $c^{(1)}$ for different values of core to tube radius a for $\mu_\mathrm{r} = 0.5$ and $H = 2$.

As shown in the table, at leading order the wavespeed $c^{(0)}$ is real and is identical to that for core-annular flow in rigid tube, similar to the earlier studies by Hickox[22] and Preziosi *et al.*[23] However, the first correction is purely imaginary and is affected by the deformability of the solid

TABLE I. Long-wave results for $\mu_\mathrm{r} = 0.5$ and $H = 2$ at different values of a.

a	$c^{(0)}$	$c^{(1)}$
0.1	0.98990	$\mathrm{i}(-1.3602 \times 10^{-6}Re + 4.5067 \times 10^{-2}\Sigma - 0.00784\Gamma)$
0.2	0.95847	$\mathrm{i}(-2.0210 \times 10^{-5}Re + 5.5552 \times 10^{-2}\Sigma - 0.11740\Gamma)$
0.3	0.90269	$\mathrm{i}(-8.6712 \times 10^{-5}Re + 5.3401 \times 10^{-2}\Sigma - 0.52378\Gamma)$
0.4	0.81903	$\mathrm{i}(-1.9466 \times 10^{-4}Re + 4.4125 \times 10^{-2}\Sigma - 1.33954\Gamma)$
0.5	0.70588	$\mathrm{i}(-2.2769 \times 10^{-4}Re + 3.1496 \times 10^{-2}\Sigma - 2.34480\Gamma)$
0.6	0.56657	$\mathrm{i}(-5.9478 \times 10^{-6}Re + 1.8834 \times 10^{-2}\Sigma - 2.94633\Gamma)$
0.7	0.41125	$\mathrm{i}(4.1462 \times 10^{-6}Re + 8.8005 \times 10^{-3}\Sigma - 2.61970\Gamma)$
0.8	0.25539	$\mathrm{i}(5.9698 \times 10^{-6}Re + 2.7445 \times 10^{-3}\Sigma - 1.51624\Gamma)$
0.9	0.11472	$\mathrm{i}(2.9115 \times 10^{-6}Re + 3.4476 \times 10^{-4}\Sigma - 0.41716\Gamma)$

TABLE II. Long-wave results for $\mu_r = 2$ and $H = 2$ at different values of a.

a	$c^{(0)}$	$c^{(1)}$
0.1	0.99005	$i(6.5539 \times 10^{-7} Re + 3.6062 \times 10^{-2}\Sigma + 0.00392\Gamma)$
0.2	0.96077	$i(8.7759 \times 10^{-6} Re + 3.9639 \times 10^{-2}\Sigma + 0.05912\Gamma)$
0.3	0.91370	$i(3.2523 \times 10^{-5} Re + 3.4191 \times 10^{-2}\Sigma + 0.27159\Gamma)$
0.4	0.85089	$i(6.3829 \times 10^{-5} Re + 2.5685 \times 10^{-2}\Sigma + 0.75101\Gamma)$
0.5	0.77419	$i(7.5613 \times 10^{-5} Re + 1.7087 \times 10^{-2}\Sigma + 1.54678\Gamma)$
0.6	0.68434	$i(4.1090 \times 10^{-5} Re + 9.9002 \times 10^{-3}\Sigma + 2.59604\Gamma)$
0.7	0.57957	$i(-4.1336 \times 10^{-5} Re + 4.7319 \times 10^{-3}\Sigma + 3.66622\Gamma)$
0.8	0.45271	$i(-1.3441 \times 10^{-4} Re + 1.6207 \times 10^{-3}\Sigma + 4.22275\Gamma)$
0.9	0.28275	$i(-1.4953 \times 10^{-4} Re + 2.4594 \times 10^{-4}\Sigma + 3.12267\Gamma)$

layer. The expression (Eq. (33)) for $c^{(1)}$ has three contributions: The term proportional to Σ is always destabilizing while the term proportional to Re is destabilizing or stabilizing depending on the value of a and μ_r. For $\mu_r = 0.5$, long-wave results show that for $a > 0.6$ (or $a < 0.6$), the first term is destabilizing (or stabilizing). The value of a below which the first term proportional to Re changes sign from positive to negative decreases with decrease in μ_r. The third term proportional to Γ in the expression of $c^{(1)}$ represents the effect of solid layer deformability on the LL interfacial mode. For $\mu_r < 1$, this term always occurs with a negative sign for all values of a, which implies that the deformability of the wall has stabilizing effect on the LL interfacial mode. When the tube walls are rigid (i.e., $\Gamma \to 0$ or $H \to 0$) and $a > 0.6$, the LL interfacial mode becomes unstable to long-wave perturbations for any nonzero value of Re and Σ. For $a < 0.6$, the relative contribution of terms proportional to Re and Σ are such that the LL interface could become unstable for Re in the range 0.1–1 and $\Sigma \gtrsim 0.1 - 1$ in a rigid tube. The long-wave asymptotic results in Table I show that for appropriately chosen nonzero values of Γ, i.e., when the tube wall is sufficiently deformable, it is possible to suppress the low wavenumber LL mode interfacial instability caused by viscosity contrast and/or capillary forces. The above results in Table I are shown for $\mu_r = 0.5$ and $H = 2$. We have verified that the qualitative nature of instability suppression due to wall deformability remains independent of H and $\mu_r < 1$.

We next consider the case when the core fluid is more viscous than the annular liquid (i.e., $\mu_r > 1$). Table II gives the values of $c^{(0)}$ and expressions for $c^{(1)}$ for different values of a for $\mu_r = 2$ and $H = 2$. The qualitative nature of the term proportional to Σ is destabilizing for $\mu_r = 2$ as well. However, the nature of other two terms in the expression of $c^{(1)}$ changes for $\mu_r = 2$ as compared to $\mu_r = 0.5$. For example, the first term proportional to Re is now stabilizing for sufficiently higher values of $a(>0.65)$ and destabilizing for lower values of $a(\leq 0.65)$. The contribution due to deformability of the wall (term proportional to Γ) is destabilizing for all values of a. For lower values of $a \leq 0.65$, the terms which are present for rigid tube, i.e., the terms proportional to Re and Σ, are destabilizing and the wall deformability (term proportional to Γ) provides additional destabilizing contribution to the LL interfacial mode. Note that for $\Gamma \to 0$ (in the limit of rigid wall) and $a > 0.65$, the LL interface remains stable when Re increases above a critical value. For example, for $a = 0.8$, the LL interface remains stable for $Re > 12.0575\Sigma$. If we fix $\Sigma = 0.1$ and $Re = 10$, this implies that the LL interfacial mode will remain stable for flow in a rigid tube. For these set of parameters ($a = 0.8$, $Re = 10$ and $\Sigma = 0.1$) and with $H = 2$, Table II shows that the value of deformability parameter Γ required to render LL interface unstable is quite low and is equal to 2.8×10^{-4}. This transition value of Γ decreases appreciably on increasing the thickness of deformable solid layer. For example, if we set $H = 5$, then the LL interface becomes unstable when Γ increases above 1.7×10^{-5}, which is an order of magnitude lower than the value of Γ at $H = 2$. Thus, these calculations show that even when the LL interface becomes stable on increasing Re in the rigid wall limit, making the walls deformable will again render the flow unstable. The results in Table II are presented for $\mu_r = 2$ and $H = 2$. However, we have verified that the destabilizing nature of wall deformability is independent of H and $\mu_r > 1$.

A. The quiescent fluid case

It is also instructive to discuss the case of a quiescent core-annular configuration of two immiscible liquids surrounded by a soft, deformable solid (i.e., the no-flow case). In the absence of the deformable solid layer, the configuration of two liquids concentrically placed inside a rigid tube becomes unstable only due to capillary forces. In the absence of flow, the wavespeed is a purely imaginary quantity, and the unstable modes are not travelling waves. Further, when there is no flow, the wavespeed $c \propto k$ for $k \ll 1$ when the outer fluid is bounded by a tube. Thus, even in the quiescent case, the destabilization of the capillary forces appear only at $O(k)$ when the tube wall is rigid, similar to CAF in a rigid tube.[22,23] It is instructive to ask whether the deformability of the soft solid layer would play a role on this capillary instability in the absence of flow. In the absence of flow, there are no neutrally stable travelling waves in the leading order, and the deformation in soft solid layer does not get affected at $O(1)$ in the asymptotic analysis. Hence, the deformability of the solid layer will not appear at $O(k)$, but only at higher orders in the analysis. Hence, it can be concluded that the deformability of the solid layer does not play a role in the quiescent case of the core-annular configuration in the limit of low k. We have verified this explicitly by carrying out a stability analysis of the quiescent case, and by analyzing the effect of the solid deformability on the growth rate of the instability both at small and finite values of k. Our results (not shown here, in the interests of brevity) indeed indicate that the deformability of the solid has an extremely weak destabilizing effect on the interfacial instability in the quiescent configuration. Thus, the stabilizing effect of the solid layer on the interfacial instability as demonstrated by our asymptotic analysis is a purely flow-induced feature.

B. Comparison with the compound-jet configuration

Another configuration that has some similarity to this work is the stability of a compound jet[52] in that the liquid-liquid interface of the inner jet is affected by another interface, viz., the gas-liquid interface (free-surface) in the compound-jet. Whereas, in the present problem, the liquid-liquid interface is affected by the dynamics of the solid-liquid interface. However, there are major differences in the consequences of the solid-liquid interface and the gas-liquid interface. In the compound-jet problem (e.g., Ref. 52), both the liquid-liquid and the gas-liquid interface are inherently unstable due to capillary forces even in the absence of flow. In the case of CAF in a deformable tube, the capillary forces are usually not strong enough to destabilize the solid-liquid interface for typical values of interfacial tension and shear modulus of the solid, with or without flow. The capillary forces will destabilize the solid-liquid interface if $\gamma_1/(GR) \sim 1$, where γ_1 is the solid-liquid interfacial tension, G is the shear modulus of the solid layer, and R is the radius of the liquid thread. As typical estimates, we use $\gamma_1 \sim 10^{-2}$ N/m, $R \sim 10^{-4}$ m, and $G \sim 10^4$ Pa, we then find $\gamma/(GR) \sim 10^{-2}$ and hence capillary forces are not strong enough to destabilize the solid-liquid interface.

In the compound-jet problem, the dynamics of the free-surface has two major effects on the liquid-liquid interface: (1) the growth rate increases by an order of magnitude when compared to the case when the annular fluid is of infinite expanse (Ref. 20), implying a strong destabilizing role, and (2) the maximum in the growth rate shifts from finite k to $k \to 0$. In the absence of flow, in contrast, the deformable solid layer has practically no effect on the capillary instability of the liquid thread as discussed in Sec. III A. The deformability of the solid plays a role only when there is flow, and the suppression or enhancement of instability of the liquid-liquid interface by the solid is purely a flow-induced effect as demonstrated by the low-k asymptotic analysis.

IV. NUMERICAL RESULTS

As discussed above and in Sec. I, the cylindrical interface between core and annular liquids becomes unstable due to capillary forces even in absence of flow. This capillary instability is independent of viscosity ratio μ_r. Preziosi *et al.*[23] have shown for core-annular flow in rigid tubes that when annular liquid is less viscous ($\mu_r > 1$) and occupies much less space than the more viscous core liquid, there exists a stability window in Re where stable core-annular flow arrangement can

be achieved. On the other hand, when annular liquid is more viscous than the core liquid ($\mu_r < 1$), no such stability window exists and the configuration is unstable. In Subsections IV A and IV B, we discuss the effect of the solid deformability for $\mu_r > 1$ and $\mu_r < 1$ separately.

A. Annular liquid is more viscous ($\mu_r < 1$)

The results in Sec. III show that the LL interfacial instability due to capillary forces and viscosity contrast can be suppressed for $k \ll 1$ when the wall deformability parameter Γ exceeds a critical value. In the following, we explore whether the predicted suppression for low wavenumber perturbations extends to finite wavenumbers as well. It is also known from the earlier works[34,38] that the LL interface could become unstable at sufficiently higher values of solid deformability parameter Γ. Moreover, there is an additional LS interface for flow in a deformable tube which could possibly become unstable upon increasing wall deformability. Indeed, it has been observed for Hagen-Poiseuille flow in a neo-Hookean deformable tube that there are upstream travelling shear waves in the solid which could be destabilized by fluid flow when the parameter Γ increases above a critical value.[40] Further, Gkanis and Kumar[32] demonstrated for flow past neo-Hookean solid that the LS interface becomes unstable for high-wavenumber perturbations when $\Gamma \sim 1$ increases above a critical value. Thus, the above discussion shows that the LL interfacial mode instability can be suppressed (for $k \ll 1$) when Γ increases above a particular value, and with further increase in Γ to higher values, both LL and LS interfaces could become unstable for sufficiently deformable walls. Consequently, we next address the question whether the predicted low-k suppression holds for finite-k as well, and whether there will be a sufficient window in terms of parameter Γ (or alternatively wall shear modulus) where both LL and LS interfaces remain stable.

In the following, we fix $\mu_r = 0.5$ for discussing the results for $\mu_r < 1$ and present neutral stability diagrams in $\Gamma - k$ plane to demarcate stable and unstable regions. Figure 2 shows the neutral stability curves in $\Gamma - k$ plane for $a = 0.9$, $Re = 1$, $\Sigma = 0.1$ and $H = 2$. In the rigid wall limit ($\Gamma \to 0$), the LL interface is unstable for nonzero values of Re and Σ (region below lower LL mode neutral curve; also see Table I). As the wall deformability parameter Γ is increased above the lower LL mode neutral curve, there is a transition from unstable to stable region for LL interfacial mode. With further increase in Γ, the LL interfacial mode becomes unstable for a band of finite wavenumber (k in the range 1–10) perturbations which is represented by the upper LL mode neutral curve. Importantly, there exists a range of values of parameter Γ between lower and upper LL mode

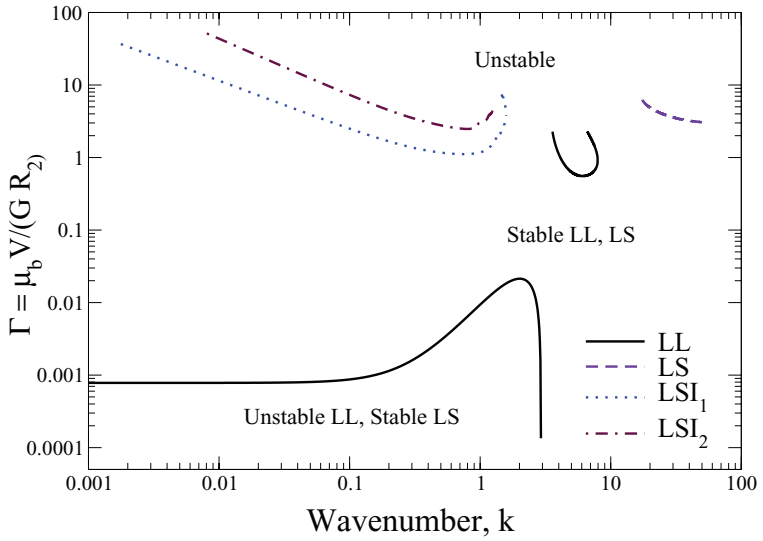

FIG. 2. Neutral stability curves in the Γ–k plane illustrating the presence of a stability window in the parameter Γ where all modes are stable: Data for $\mu_r = 0.5$, $a = 0.9$, $H = 2$, $Re = 1$, $\Sigma = 0.1$, $\Sigma_1 = 0$, $\eta_r = 0$.

neutral curves where both LL and LS interfaces remain stable. We have used a pseudo-spectral collocation method, which does not require any initial guess for the eigenvalues, and provides a truncated version of the eigenspectrum of the problem. As we increase the number of polynomials used for the expansion, the number of eigenvalues increase, but the additional eigenvalues are always stable. Thus, the pseudo-spectral method can capture all the relevant (i.e., unstable) eigenvalues, and we have verified that no new unstable mode occurs with increase in the number of polynomials. We used the spectral code to ensure that there are no unstable modes in the region between lower and upper LL mode neutral curves in Figure 2. Thus, there exists a stability window in terms of parameter Γ ($0.021 < \Gamma < 0.55$) where stable core-annular flow arrangement of two liquids could be achieved by using a deformable solid coating, which was otherwise unstable for flow in a rigid tube. For the data set used in Figure 2, the stability window is determined by lower and upper LL mode neutral curves. However, at higher values of Γ, the LS interface could also become unstable and we will show a little later that depending on the parameters, the stability window is determined by lower LL and upper LL or LS mode neutral curves.

In Figure 2, when Γ is increased to sufficiently high values, we encounter a set of neutral curves which correspond to the instability of liquid-solid interface. For example, the two neutral curves shown by dotted and dashed-dotted lines belong to the class of low-*Re* low-k LS interfacial mode predicted by Gaurav and Shankar[40] for Hagen-Poiseuille flow in a neo-Hookean deformable tube. Gaurav and Shankar[40] analyzed the stability of Hagen-Poiseuille flow in an elastic neo-Hookean tube and demonstrated that there exist multiple upstream travelling shear waves in the solid which becomes unstable in presence of inertia when the deformability parameter Γ increases beyond a critical value. In the low-*Re*, low-k limit, $\Gamma \sim 1$, $k \sim Re^{1/2}$ and $c_r \sim Re^{-1}$ for these unstable modes. We have verified this scaling behavior for the two neutral curves shown by dotted and dashed-dotted lines in Figure 2. Since inertia is necessary for the presence of these unstable modes, we refer these unstable modes as inertial LS (LSI) modes in the present work. Only the two most unstable inertial modes are shown in Figure 2. The other higher inertial modes become unstable at very high values of Γ and are not relevant in the context of present study. The neutral curve shown on the right side of Figure 2 by dashed line depicts the short-wave instability of LS interface which was first predicted by Gkanis and Kumar[32] for plane Couette flow past neo-Hookean elastic surface. This high-wavenumber instability is caused by the nonzero first normal stress difference in the base state present for a neo-Hookean solid model.

Figure 3 compares the neutral stability curves for two different values of solid thickness. In Figure 3, only those neutral curves are presented which are critical for determining the width of stability window for a given solid thickness. For $H = 2$, the stable gap is determined by lower and

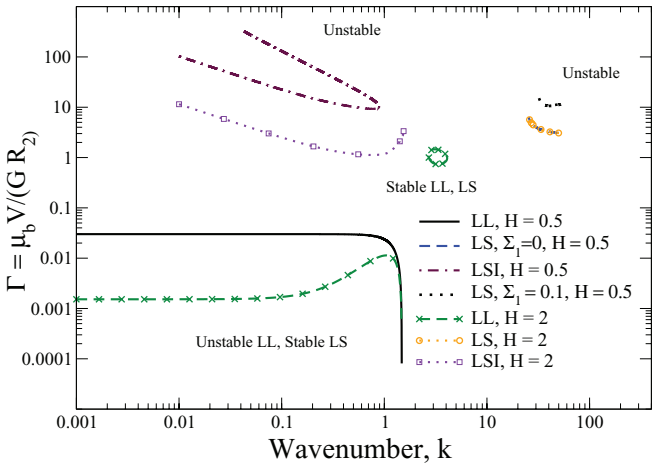

FIG. 3. Neutral stability curves in the Γ–k plane illustrating the increase in width of stability window at lower solid thickness: Data for $\mu_r = 0.5$, $a = 0.9$, $Re = 1$, $\Sigma = 1$, $\eta_r = 0$. Combination of different line-styles and symbols are used for $H = 2$ while only different line-styles are used for $H = 0.5$.

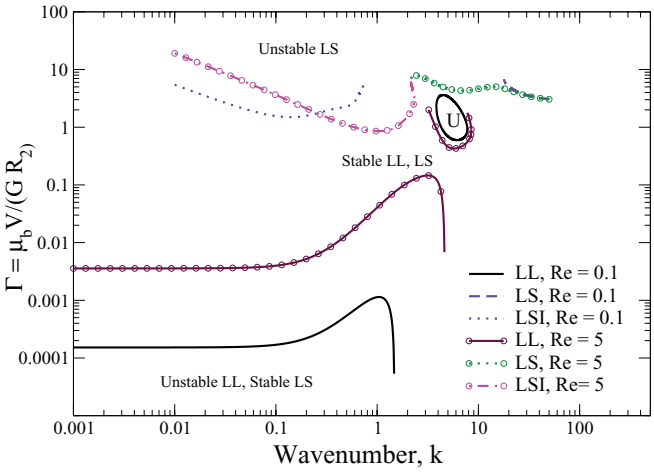

FIG. 4. Neutral stability curves in the Γ–k plane showing the effect of varying Re on stability window: Data for $\mu_r = 0.5$, $a = 0.9$, $H = 2$, $\Sigma = 0.1$, $\Sigma_1 = 0$, $\eta_r = 0$. Combination of different line-styles and symbols are used for $Re = 5$ while only different line-styles are used for $Re = 0.1$.

upper LL mode neutral curves. The lower LL mode neutral curve shows that the critical Γ required for transition from unstable to stable region is around 0.01. The upper LL mode neutral curve shows that the LL interface again becomes unstable when Γ increases beyond 0.75. On the other hand, the width of stable region for $H = 0.5$ is determined by lower LL and short-wave LS mode neutral curves. The critical values for these two modes are 0.03 and 3, respectively. Thus, there is an order of magnitude increase in the width of stability window with sufficient decrease in solid thickness. Thus, for fixed flow parameters and fluid properties, the width of stable region can be increased by decreasing the thickness of solid layer. It is important to point out that the LL interfacial tension parameter $\Sigma = 1$ for data presented in Figure 3. We have verified that the upper LL mode neutral curve vanishes for $H = 0.5$ on increasing Σ from 0.1 to 1. It is because of this absence of upper LL mode neutral curve at a higher value of $\Sigma = 1$, that the stable gap for $H = 0.5$ is determined by lower LL and short-wave LS mode neutral curves. For lower values of $\Sigma \sim 0.1$, the upper LL mode neutral curve exists for $H = 0.5$ as well. The stable region is then determined by lower and upper LL mode neutral curves for $H = 0.5$ and the width of stability window is almost same for both $H = 0.5$ and $H = 2$. Figure 3 also shows the effect of increasing LS interfacial tension parameter on the short-wave LS mode. We have verified that the LS interfacial tension does not affect the neutral curves for LL and inertial LS modes. It is also important to mention here that the short-wave LS mode neutral curve remains independent of solid thickness.[32] Figure 3 shows that the short-wave LS mode is highly stabilized on increasing Σ_1 from 0 to 0.1 and the critical Γ required for exciting the high wavenumber instability increases from 3 to 10. For $H = 0.5$ and $\Sigma_1 = 0.1$, the lower LL and inertial LS or short-wave LS modes determine the width of stable region. The width of stability window increases by an order of magnitude for $\Sigma_1 = 0.1$ as compared to $\Sigma_1 = 0$ for $H = 0.5$. Thus, this figure shows that stability gap can be significantly increased for sufficiently lower solid thicknesses by increasing the LS interfacial tension.

Figure 4 depicts the neutral stability curves for two different values of Reynolds numbers. For both $Re = 0.1$ and $Re = 5$, the stable region is determined by the lower and upper LL mode neutral curves. It is evident from Figure 4 that the critical value of Γ required for destabilization of LL mode (the minimum of upper LL mode neutral curve) is not significantly affected by increase of Re from 0.1 to 5. However, the lower LL mode neutral curves show that the value of Γ above which there is a transition from unstable LL to stable LL perturbations is almost two order of magnitudes larger for $Re = 5$ as compared to $Re = 0.1$. As a result, there is a much wider stability window at lower Reynolds number (e.g., at $Re = 0.1$ in Figure 4) and with increase in Re the width of stability region decreases. For the set of parameters in Figure 4, we have verified that the width of stability

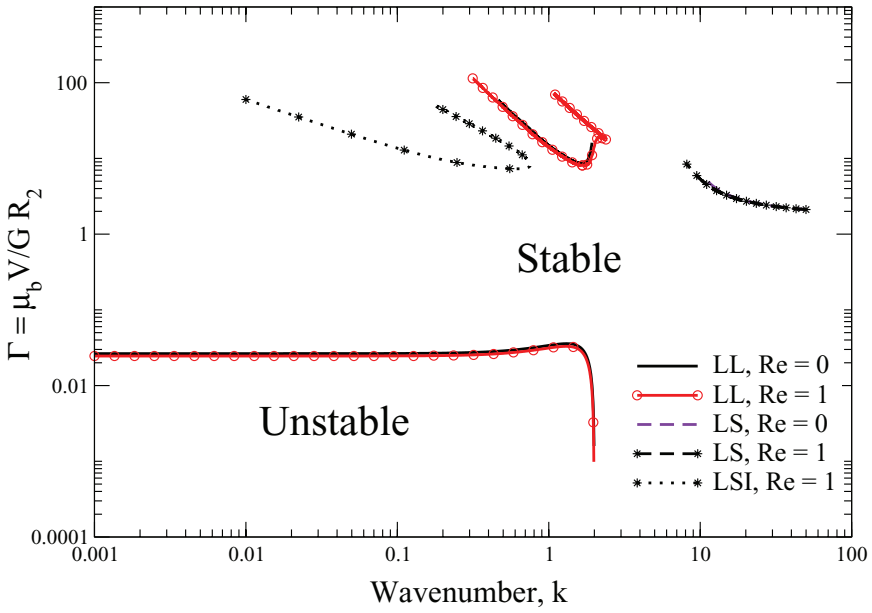

FIG. 5. Neutral stability curves in the Γ–k plane: Data for $\mu_r = 0.5$, $a = 0.5$, $H = 0.5$, $\Sigma = 0.1$, $\Sigma_1 = 0$, $\eta_r = 0$. Combination of different line-styles and symbols are used for $Re = 1$ while only different line-styles are used for $Re = 0$.

window vanishes for $Re \sim 10$ and stable core-annular flow arrangement in a deformable tube could be achieved only for $Re \lesssim 1$.

All the numerical results presented thus far are for $a = 0.9$, i.e., when the annular liquid occupies much less space than the core liquid. We have also verified the existence of stability window for $a = 0.7$, $Re \lesssim 1$ and $\Sigma \sim 0.1 - 1$. The results for $a = 0.7$ are qualitatively similar to the results shown in Figures 2–4 for $a = 0.9$. The low-k results in Table I show that the contribution of term proportional to Re changes qualitatively with decrease in mean LL interface position. For example, Table I shows that for $a = 0.5$, the term proportional to Re becomes stabilizing and the term proportional to Σ remains destabilizing. Figure 5 shows the neutral stability curves for $a = 0.5$ and it shows the existence of sufficiently wide stability window for both $Re = 0$ and 1. The only difference between neutral curves at $Re = 0$ and $Re = 1$ is the existence of inertial LS modes at $Re = 1$. Figure 5 shows that the lower LL and short-wave LS mode determine the stability window. The value of $\Sigma_1 = 0$ in Figure 5 and as discussed earlier that the nonzero values of Σ_1 will have a stabilizing effect on the short-wave LS mode. Thus, for nonzero values of LS interfacial tension, the stability gap will increase and depending on parameters, the width of stability window will be determined by lower LL and inertial LS or upper LL mode neutral curves. Note that, even though the contribution proportional to Re is stabilizing in low-k limit, the lower LL mode neutral curve, which gives transition value of Γ for stabilizing LL interface, remains almost identical for both $Re = 0$ and 1. This is because the stabilizing contribution due to inertia is much weaker than the destabilizing contribution due to surface tension forces. We have verified this by plotting c vs. k data for $Re = 0$ and 1 in the rigid limit ($H = 0$) as well as for different values of H and Γ. The c_i vs. k data (not shown) illustrate that the changes in growth rates are very small on increasing Re from 0 to 1. This is also evident from low-k results for $a = 0.5$ in Table I. Since the contribution proportional to Re (term present because of viscosity contrast) is stabilizing, the neutral stability data in Figure 5 essentially show the stabilization of capillary instability of liquid-liquid interface due to wall deformability.

Figure 6 shows neutral stability curves for $a = 0.3$, $Re = 0$, and $\Sigma = 0.1$. Similar to $a = 0.5$, the effect of Σ is destabilizing while the term proportional to Re is stabilizing in the low-k limit. Therefore, we set $Re = 0$ to suppress this stabilizing effect and focus entirely on the effect of tube wall deformability on the capillary instability. Figure 6 for $a = 0.3$ and $\Sigma = 0.1$ illustrates that while the LL mode perturbations with $k \ll 1$ are suppressed upon increasing Γ above a threshold value,

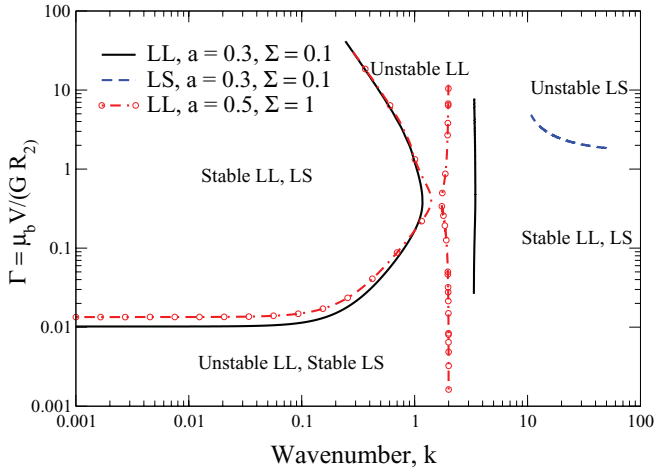

FIG. 6. Neutral stability curves in $\Gamma - k$ plane: Data for $\mu_r = 0.5$, $a = 0.3$ and 0.5, $H = 2$, $Re = 0$, $\Sigma = 0.1$, $\Sigma_1 = 0$, $\eta_r = 0$ show that solid deformability is unable to completely suppress the capillary instability at all wavenumbers.

it is not possible to suppress perturbations with $k \sim 1$ by changing the deformability of the tube wall. There exists a band of wavenumbers with $k \approx 1-3$ where the LL interface is unstable because of capillary instability and hence, complete stabilization is not possible. This is in contrast to the results presented thus far for $a = 0.5$ and $\Sigma = 0.1$ (Figure 5) and other values of a, where a stability window (at all values of k) in terms of parameter Γ was always observed. For $a = 0.3$, the strong destabilizing capillary forces dominate over the wall deformability effect and hence stabilization of LL interface could not be achieved. This strong capillary instability is of course expected for lower values of mean LL interface position. Figure 6 also reports data for $a = 0.5$ at higher value of $\Sigma = 1$ as compared to $\Sigma = 0.1$ in Figure 5. A comparison of data in Figures 5 and 6 for $a = 0.5$ show that the stability window ceases to exist as Σ is increased from 0.1 to 1. We also investigated the effect of Σ for different values of a and observed the presence of stable gap at $a = 0.9$ for Σ values as high as 10. On the other hand, for $a = 0.6$, stable gap vanishes when Σ is increased from 2 to 4.5. Thus, for $Re \sim 1$, the existence of stability window depends on the competition between the destabilizing capillary forces and stabilizing effect of wall deformability. The above discussion suggests that it is possible to obtain stable core-annular flow arrangement by tuning wall deformability for sufficiently higher values of a. However, stabilization of capillary instability is not possible for lower values of mean LL interface position. Even though stabilization of LL interface is not possible for $a = 0.3$, a feature worth noting in Figure 6 is that only a selective band of wavenumbers $k \approx 1-3$ become unstable for core-annular flow in a deformable tube. This range is more selective with $a = 0.5$ and $\Sigma = 1$. This is in contrast with core-annular flow in a rigid tube where perturbation with all wavenumbers below $k \sim 1$ become unstable. Thus, it is possible to excite perturbations with selective wavelength for flow in a deformable tube. This feature could be potentially exploited to provide tighter control in microfluidic devices which are used to produce uniform sized droplets.

All the results presented thus far are for purely elastic neo-Hookean solid with $\eta_r = 0$. Figure 7 shows the effect of solid viscosity η_r on different neutral stability curves. It clearly demonstrates that the lower LL mode neutral curve remains exactly identical with increase in η_r above zero and hence, the transition value of Γ above which the LL interface becomes stable is not affected by varying solid viscosity. In contrast, the solid viscosity has stabilizing effect on upper LL mode neutral curve. Figure 7 shows that unstable region shrinks on increasing η_r from 0 to 0.3 and finally vanishes at $\eta_r = 0.5$. The effect of solid viscosity is even more dramatic on inertial LS modes. Figure 7 shows that area of unstable region for inertial LS modes decreases significantly and forms an island of instability for η_r as low as 0.02. With further increase in η_r, this unstable region shrinks rapidly and finally vanishes for $\eta_r \gtrsim 0.03$. This strong stabilizing effect of solid viscosity on inertial LS modes was also observed in Hagen-Poiseuille flow of a single fluid in a neo-Hookean viscoelastic tube.[40] As a consequence of stabilization of upper LL and inertial LS mode neutral curves beyond

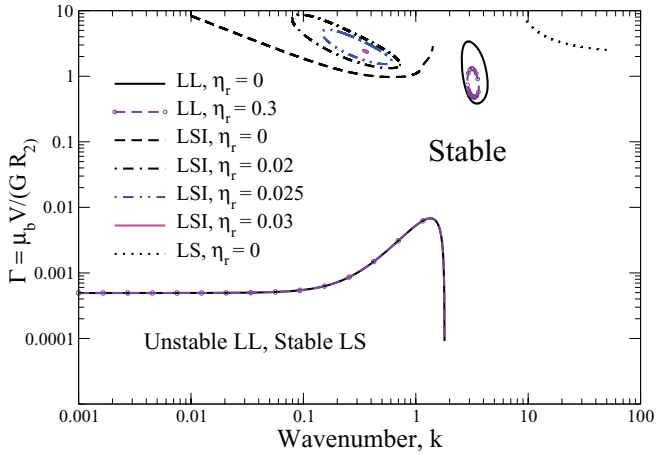

FIG. 7. Neutral stability curves in $\Gamma - k$ plane: Data for $\mu_r = 0.5$, $a = 0.7$, $H = 2$, $Re = 1$, $\Sigma = 0.1$, $\Sigma_1 = 0$ show the effect of solid viscosity on the CAF instability.

a critical η_r, the stability window is determined by lower LL and short-wave LS mode neutral curves. This results in a wider stable gap in terms of parameter Γ with nonzero η_r. However, for the parameter sets where capillary instability dominates and stability window does not exist (for example, $a = 0.5$, $\Sigma = 1$ and for lower values of a), it is still not possible to obtain stable gap using nonzero η_r.

We end this section by providing some estimates of the dimensional parameters where the predicted suppression of instability may be realized in experiments. The above results show that a stable flow arrangement could be obtained at higher values of a for $Re \lesssim 1$ and $\Sigma \lesssim 1$. If we set $\rho \sim 10^3$ kg/m^3, $R_2 \sim 10^{-4}$ m, and $\sigma \sim 0.01$ N/m, then $Re \sim 0.1$ and $\Sigma \sim 1$ correspond to $\mu_b \sim 0.1$Pa s and centerline velocity $V \sim 0.1$ m/s. Our results (e.g., Fig. 7) show that $\Gamma \gtrsim 0.001$ to obtain stable flow arrangement. This corresponds to the shear modulus values of $G \lesssim 10^5$ Pa. Thus, the predicted suppression of instability is realizable for systems involving very viscous liquids flowing past soft deformable solid wall.

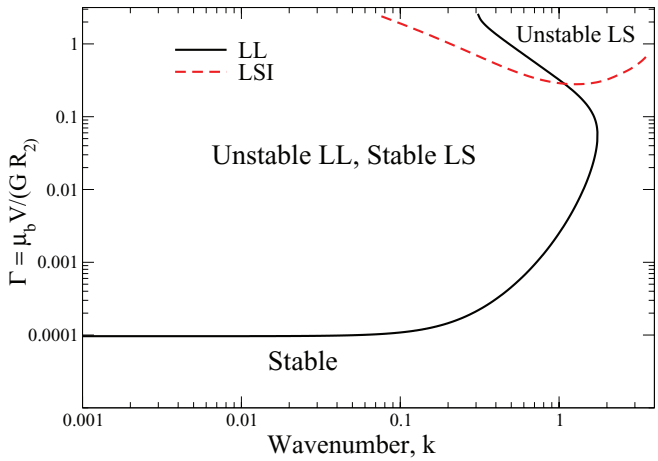

FIG. 8. Neutral stability curves in $\Gamma - k$ plane showing destabilizing role of wall deformability. Data for $\mu_r = 2$, $a = 0.7$, $H = 2$, $Re = 20$, $\Sigma = 0.1$, $\Sigma_1 = 0$, $\eta_r = 0$.

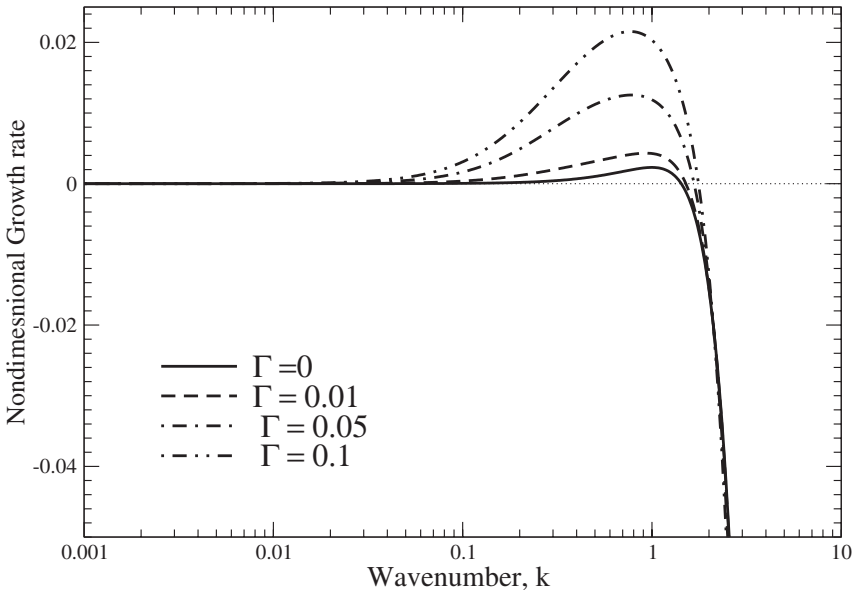

FIG. 9. Growth rate curves in $\Gamma - k$ plane illustrating destabilizing role of wall deformability. Data for $\mu_r = 2$, $a = 0.7$, $H = 2$, $Re = 0$, $\Sigma = 1.0$, $\Sigma_1 = 0$.

B. Core liquid is more viscous ($\mu_r > 1$)

We next examine the role of wall deformability for $\mu_r > 1$. Preziosi *et al.*[23] demonstrated that it is possible to obtain stable core-annular flow in a rigid tube when *Re* remains in between a lower and upper limit. For $\mu_r = 2$, $a = 0.7$ and $\Sigma = 0.1$, this lower and upper limit of *Re* is approximately 11.5 and 120 for flow in a rigid tube ($\Gamma \to 0$). Figure 8 shows the neutral stability data for $\mu_r = 2$, $a = 0.7$ and $\Sigma = 0.1$ with $H = 2$ and $Re = 20$. This figure illustrates that the configuration remains stable in the rigid limit ($\Gamma \to 0$) and with increase in Γ beyond a critical value, the LL interface becomes unstable for perturbations with $k \lesssim 1$. With further increase in Γ, the LS interface also becomes unstable as was also observed for $\mu_r < 1$. However, for $\mu_r = 2$, and above a critical nonzero Γ (i.e., with deformable tube wall), there is no region in $\Gamma - k$ plane where both interfaces simultaneously remain stable. Thus, a configuration which remains stable in the rigid limit can be rendered unstable by making the walls sufficiently deformable. Further, Figure 9 shows growth rate vs. wavenumber data for $H = 2$, $Re = 0$ and $\Sigma = 1$ at different values of Γ. In this figure, we set $Re = 0$ to suppress stabilizing inertial effects and compare the relative magnitude of destabilizing contributions due to interfacial tension and wall deformability. Figure 9 shows that the rate of growth of perturbations is always higher for the case of deformable tube as compared to the rigid limit ($\Gamma \to 0$). In fact, the maximum growth rate for flow in a rigid tube is around 0.001, while for $\Gamma \sim 0.1$, the maximum growth rate is around 0.01 which is an order of magnitude higher than growth rate in the rigid limit. This result shows that the rate of growth of perturbations can be appreciably increased by increasing wall deformability and it is expected that the instability will set in rapidly in deformable tube as compared to flow in a rigid tube. This feature could be potentially used either for rapidly mixing the fluid streams in microchannels which are often fabricated using soft elastomers like PDMS, or for expediting drop formation in microfluidic devices.

V. CONCLUSIONS

The stability of core-annular flow of two immiscible fluids surrounded by an annular, deformable solid layer was analyzed using low-wavenumber asymptotic analysis and numerical solutions valid at arbitrary wavenumbers by considering axisymmetric modes of disturbances. For core-annular flow in a rigid tube, the liquid-liquid interface is generally unstable if the more viscous fluid is in

the annulus, while it could be stable or unstable if the less viscous fluid is in the annular region (depending on the thickness of the less viscous fluid). In addition to instability of the interface due to viscosity stratification (which is also present in the case of planar two-layer flows[21]), the capillary instability mechanism plays an important, and even dominant role in the stability of CAFs. Our low-wavenumber analysis shows that deformability of the solid layer always has a stabilizing (destabilizing) effect if the more viscous fluid is in the annular (core) region. Thus, the effect of the solid layer deformability is quite opposite to the effect of viscosity-stratification, while the capillary mechanism always acts to destabilize the liquid-liquid interface. Consequently, the stability of the CAF inside a deformable tube is governed by a competition between these three distinct mechanisms. When the more viscous fluid is in the annular region, our asymptotic results show that by decreasing the shear modulus of the solid it is possible to suppress the instability of LL interface at low wavenumbers. To verify whether this suppression extends to disturbances of arbitrary wavenumbers, we solved the coupled linearized governing equations numerically. Our numerical results show that the low-wavenumber prediction of suppression under increased solid deformability indeed carries over to finite wavenumbers. However, as the solid becomes more deformable, the LL and the LS interfaces could become unstable at finite wavelengths. Thus, it is necessary to establish that there exists an intermediate "window" in the values of shear modulus of the soft solid layer wherein the LL and LS interfaces are stable at all wavenumbers. Our numerical results show that it is possible to tune the shear modulus, thickness, and the viscosity of the solid layer to obtain such a window of shear moduli where the system is stable at all wavenumbers. We also illustrated that the stabilizing nature of the deformable solid is seen only if there is a flow, and the deformability of the solid has very little effect on the liquid-liquid interface when the system is quiescent. When the annular fluid is less viscous, our results show that the effect of solid deformability is always destabilizing. The predicted influence of solid layer deformability on the instability of the interface in a CAF can be potentially exploited in microfluidic flows designed to produce tiny mono-disperse droplets. In such applications, it would be desirable to have control on the formation of drops, such as the spatial location of the instability inside the microfluidic device. This can be achieved by fabricating PDMS-based channels with spatially varying shear modulus, by tuning the shear modulus values such that initially the CAF is stable, while the CAF is unstable at the desired location. Our estimates show that the predicted effects of the deformable solid layer will occur typically in microfluidic channels of diameter 10^{-4} m, flow velocity $V \sim 0.1$ m/s, annular fluid viscosity $\mu \sim 10^{-1}$ kg/m s and with shear modulus of the solid layer $G \lesssim 10^5$ Pa.

ACKNOWLEDGMENTS

We wish to acknowledge assistance from Ms. Hemalatha Annepu in formulating the pseudo-spectral code.

APPENDIX: ANALYTICAL EXPRESSIONS FOR $c^{(0)}$ AND $c^{(1)}$

In this Appendix, we provide the analytical expressions for $c^{(0)}$ and $c^{(1)}$ discussed in Sec. III

$$c^{(0)} = \left[\frac{\mu_r(a^2-1)}{a^4(\mu_r-1)-\mu_r}\right],$$

$$c^{(1)} = \mathrm{i}(f_2\Sigma + f_3\Gamma + f_1 Re),$$

$$f_2 = \frac{a}{16}\left[\frac{(a^2-1)(1-4\mu_r+a^2(4\mu_r-3))}{a^4(\mu_r-1)-\mu_r} - 4\log[a]\right],$$

$$f_3 = -\left[\frac{Ha^4(a^2-1)^2(4+6H+4H^2+H^3)(\mu_r-1)\mu_r^2}{(a^4(\mu_r-1)-\mu_r)^3}\right],$$

$$f_1 = \frac{-a^4\mu_1}{144}\left[\frac{-(a^2-1)(r_1-r_2+r_3-r_4)+r_5r_6\log[a]}{D}\right],$$

$$r_1 = a^2(9 - 16\mu_r)\mu_r^3 + 2\mu_r^4 + a^8\mu_1\mu_r(87 - 362\mu_r + 286\mu_r^2),$$

$$r_2 = 5a^6\mu_1\mu_r(3 + 8\mu_r(-3 + 4\mu_r)) + a^4\mu_r^2(12 + \mu_r(-53 + 46\mu_r)),$$

$$r_3 = a^{12}{\mu_1}^2(21 + \mu_r(-63 + 50\mu_r)),$$

$$r_4 = a^{10}{\mu_1}^2(9 + \mu_r(-159 + 208\mu_r)),$$

$$r_5 = 24a^6(a^4\mu_1 - \mu_r)\mu_1,$$

$$r_6 = \left[-6a^2\mu_1\mu_r + (-1 + 2\mu_r)(a^4\mu_1 + 2\mu_r)\right],$$

$$D = (a^4\mu_1 - \mu_r)^3(\mu_r - a^2\mu_1),$$

$$\mu_1 = (1 - \mu_r).$$

[1] D. Joseph and Y. Renardy, *Fundamentals of Two-Fluid Dynamics: Part 1: Mathematical Theory and Applications* (Springer-Verlag, New York, 1993).
[2] D. D. Joseph, R. Bai, K. P. Chen, and Y. Y. Renardy, "Core-annular flows," Annu. Rev. Fluid Mech. **29**, 65 (1997).
[3] J. B. Grotberg, "Respiratory fluid mechanics," Phys. Fluids **23**, 021301 (2011).
[4] D. Halpern and J. B. Grotberg, "Fluid-elastic instabilities of liquid-lined flexible tubes," J. Fluid Mech. **244**, 615 (1992).
[5] D. Halpern and J. B. Grotberg, "Surfactant effects on fluid-elastic instabilities of liquid-lined flexible tubes: A model of airway closure," J. Biomech. Eng. **115**, 271 (1993).
[6] P. Garstecki, H. A. Stone, and G. M. Whitesides, "Mechanism for flow-rate controlled breakup in confined geometries: A route to monodisperse emulsions," Phys. Rev. Lett. **94**, 164501 (2005).
[7] A. S. Utada, A. Fernandez-Nieves, H. A. Stone, and D. A. Weitz, "Dripping to jetting transitions in coflowing liquid streams," Phys. Rev. Lett. **99**, 094502 (2007).
[8] A. S. Utada, A. Fernandez-Nieves, J. M. Gordillo, and D. A. Weitz, "Absolute instability of a liquid jet in a coflowing stream," Phys. Rev. Lett. **100**, 014502 (2008).
[9] P. Guillot, A. Colin, and A. Ajdari, "Stability of a jet in confined pressure-driven biphasic flows at low Reynolds number in various geometries," Phys. Rev. E **78**, 016307 (2008).
[10] A. S. Utada *et al.*, "Monodisperse double emulsions generated from a microcapillary device," Science **308**, 537 (2005).
[11] A. S. Utada *et al.*, "Dripping, jetting, drops, and wetting: The magic of microfluidics," MRS Bull. **32**, 702 (2007).
[12] K. J. Humphry *et al.*, "Suppression of instabilities in multiphase flow by geometric confinement," Phys. Rev. E **79**, 056310 (2009).
[13] H.-H. Wei and D. S. Rumschitzki, "The effect of insoluble surfactants on the linear stability of a core-annular flow," J. Fluid Mech. **541**, 115 (2005).
[14] H.-H. Wei, "Marangoni destabilization on a core-annular film flow due to the presence of a surfactant," Phys. Fluids **17**, 027101 (2005).
[15] M. G. Blyth and C. Pozrikidis, "Stability of axisymmetric core annular flow in the presence of an insoluble surfactant," J. Fluid Mech. **548**, 207 (2006).
[16] A. P. Bassom, M. G. Blyth, and G. T. Papageorgiou, "Using surfactants to stabilize two-phase pipe flows of core-annular type," J. Fluid Mech. **704**, 333 (2012).
[17] J. C. McDonald and G. M. Whitesides, "Poly(dimethylsiloxane) as a material for fabricating microfluidic devices," Acc. Chem. Res. **35**, 491 (2002).
[18] L. Rayleigh, *Theory of Sound*, 2nd ed. (Dover, New York, 1945).
[19] S. Chandrasekhar, *Hydrodynamic and Hydromagnetic Stability* (Dover, New York, 1981).
[20] S. Tomotika, "On the instability a cylindrical thread of a viscous liquid surrounded by another viscous fluid," Proc. R. Soc. London, Ser. A **150**, 322 (1935).
[21] C.-S. Yih, "Instability due to viscosity stratification," J. Fluid Mech. **27**, 337 (1967).
[22] C. E. Hickox, "Instability due to viscosity and density stratification in axisymmetric pipe flow," Phys. Fluids **14**, 251 (1971).
[23] L. Preziosi, K. Chen, and D. D. Joseph, "Lubricated pipelining: stability of core-annular flow," J. Fluid Mech. **201**, 323 (1989).
[24] P. A. M. Boomkamp and R. H. M. Miesen, "Nonaxisymmetric waves in core-annular flow with a small viscosity ratio," Phys. Fluids **4**, 1627 (1992).
[25] H. H. Hu and N. Patankar, "Non-axisymmetric stability of core-annular flow," J. Fluid Mech. **290**, 213 (1995).
[26] Y. Y. Renardy, "Snakes and corkscrews in core-annular down-flow of two fluids," J. Fluid Mech. **340**, 297 (1997).
[27] S. Kwak and C. Pozrikidis, "Effect of surfactants on the instability of a liquid thread or annular layer. Part I. Quiescent fluids," Int. J. Multiphase Flow **27**, 1 (2001).
[28] B. Selvam, S. Merk, R. Govindarajan, and E. Meiburg, "Stability of miscible core-annular flow with viscosity stratification," J. Fluid Mech. **592**, 23 (2007).
[29] P. Guillot, A. Colin, A. S. Utada, and A. Ajdari, "Stability of a jet in confined pressure-driven biphasic flows at low Reynolds numbers," Phys. Rev. Lett. **99**, 104502 (2007).

[30] V. Kumaran, G. H. Fredrickson, and P. Pincus, "Flow induced instability of the interface between a fluid and a gel at low Reynolds number," J. Phys. II (France) **4**, 893 (1994).
[31] V. Kumaran and R. Muralikrishnan, "Spontaneous growth of fluctuations in the viscous flow of a fluid past a soft interface," Phys. Rev. Lett. **84**, 3310 (2000).
[32] V. Gkanis and S. Kumar, "Instability of creeping Couette flow past a neo-Hookean solid," Phys. Fluids **15**, 2864 (2003).
[33] M. D. Eggert and S. Kumar, "Observations of instability, hysteresis, and oscillation in low-Reynolds number flow past polymer gels," J. Colloid Interface Sci. **278**, 234 (2004).
[34] V. Shankar and L. Kumar, "Stability of two-layer Newtonian plane Couette flow past a deformable solid layer," Phys. Fluids **16**, 4426 (2004).
[35] V. Shankar and A. K. Sahu, "Suppression of instability in liquid flow down an inclined plane by a deformable solid layer," Phys. Rev. E **73**, 016301 (2006).
[36] Gaurav and V. Shankar, "Stability of gravity-driven free-surface flow past a deformable solid layer at zero and finite Reynolds number," Phys. Fluids **19**, 024105 (2007).
[37] A. Jain and V. Shankar, "Elastohydrodynamic suppression of free-surface instabilities in annular liquid film flow outside wires and inside tubes," Ind. Eng. Chem. Res. **47**, 6473 (2008).
[38] Gaurav and V. Shankar, "Role of wall deformability on interfacial instabilities in gravity-driven two-layer flow with a free surface," Phys. Fluids **22**, 094103 (2010).
[39] V. Kumaran, "Stability of the viscous flow of a fluid through a flexible tube," J. Fluid Mech. **294**, 259 (1995).
[40] Gaurav and V. Shankar, "Stability of fluid flow through deformable neo-Hookean tubes," J. Fluid Mech. **627**, 291 (2009).
[41] R. L. Fosdick and J. H. Yu, "Thermodynamics, stability and non–linear oscillations of viscoelastic solids – I. Differential type solids of second grade," Int. J. Non-Linear Mech. **31**, 495 (1996).
[42] M. A. Hayes and G. Saccomandi, "Finite–amplitude waves superimposed on pseudoplanar motions for Mooney–Rivlin viscoelastic solids," Int. J. Non-Linear Mech. **37**, 1139 (2002).
[43] M. Destarde and G. Saccomandi, "Finite-amplitude inhomogeneous waves in Mooney–Rivlin viscoelastic solids," Wave Motion **40**, 251 (2004).
[44] L. E. Malvern, *Introduction to the Mechanics of a Continuous Medium* (Prentice-Hall, Englewood Cliffs, NJ, 1969).
[45] G. A. Holzapfel, *Nonlinear Solid Mechanics* (Wiley, Chichester, 2000).
[46] Gaurav and V. Shankar, "Stability of pressure-driven flow in a deformable neo-Hookean channel," J. Fluid Mech. **659**, 318 (2010).
[47] J. P. Boyd, *Chebyshev and Fourier Spectral Methods*, 2nd ed. (Dover, New York, 2001).
[48] J. A. Weideman and S. C. Reddy, "A MATLAB differentiation matrix suite," ACM Trans. Math. Softw. **26**, 465 (2000).
[49] W. Huang and D. M. Sloan, "The pseudospectral method for solving differential eigenvalue problems," J. Comput. Phys. **111**, 399 (1994).
[50] P. Drazin and W. Reid, *Hydrodynamic Stability* (Cambridge University Press, Cambridge, 1981).
[51] P. A. M. Boomkamp, B. J. Boersma, R. H. M. Miesen, and G. V. Beijnon, "A Chebyshev collocation method for solving two-phase flow stability problems," J. Comput. Phys. **132**, 191 (1997).
[52] A. Chauhan, C. Maldarelli, D. T. Papageorgiou, and D. S. Rumschitzki, "Temporal instability of compound threads and jets," J. Fluid Mech. **420**, 1 (2000).